REPORT

METALLURGY

Tracking the sliding of grain boundaries at the atomic scale

Lihua Wang[1]†, Yin Zhang[2]†, Zhi Zeng[2], Hao Zhou[2], Jian He[3], Pan Liu[4], Mingwei Chen[5], Jian Han[6], David J. Srolovitz[7,13], Jiao Teng[8], Yizhong Guo[1], Guo Yang[1], Deli Kong[1], En Ma[9], Yongli Hu[10], Baocai Yin[10], XiaoXu Huang[11], Ze Zhang[1,12]*, Ting Zhu[2]*, Xiaodong Han[1]*

Grain boundaries (GBs) play an important role in the mechanical behavior of polycrystalline materials. Despite decades of investigation, the atomic-scale dynamic processes of GB deformation remain elusive, particularly for the GBs in polycrystals, which are commonly of the asymmetric and general type. We conducted an in situ atomic-resolution study to reveal how sliding-dominant deformation is accomplished at general tilt GBs in platinum bicrystals. We observed either direct atomic-scale sliding along the GB or sliding with atom transfer across the boundary plane. The latter sliding process was mediated by movements of disconnections that enabled the transport of GB atoms, leading to a previously unrecognized mode of coupled GB sliding and atomic plane transfer. These results enable an atomic-scale understanding of how general GBs slide in polycrystalline materials.

Grain boundaries (GBs) are interfaces that separate grains of different crystal orientations (*1*, *2*). A GB slides when the two adjoining grains undergo a relative displacement parallel to the boundary plane. GB sliding, sometimes coupled with GB migration, can strongly affect the inelastic deformation of polycrystalline materials, such as diffusional creep at elevated temperature (*3*, *4*) and plastic deformation at ambient temperature (*5*–*7*). GB sliding has recently received considerable attention in studies of plastic deformation and grain size stabilization in nanocrystalline metals (*7*–*12*). Although GB-mediated deformation has been investigated using a variety of in situ and ex situ experimental techniques (*13*–*18*), the atomic-scale process by which GBs slide remains unclear, largely because of a lack of direct high-resolution, experimental observations. The past several years have seen rapid progress in in situ atomic-resolution experiments (*19*–*23*). However, the atomic-scale processes associated with the deformation of general GBs has not been clearly resolved, mainly because tracking atomic movements during GB deformation is extremely difficult.

Atomistic modeling and simulations have provided most of our current understanding of the atomic-scale events accompanying GB deformation (*4*–*7*). For example, molecular dynamics (MD) simulations have examined the mechanical behavior of special types of coincident site lattice tilt GBs in face-center cubic (FCC) bicrystals (*5*–*7*). These simulations revealed a strong coupling between GB sliding and migration through transformations of structural units between the GB and the adjoining crystal lattices (*4*–*7*), which permit sliding with no change in GB structure. This concept has been generalized to account for general GB bicrystallography and the motion of deformation-carrying line defects in GBs, i.e., disconnections (*6*, *7*). Disconnections are characterized by both a step height and Burgers vector: If the step height is zero, then the disconnection is a pure dislocation, whereas if it has zero Burgers vector, then the disconnection is a pure step. MD simulations also demonstrate that the deformation of general GBs, when mediated by GB disconnection motion at room temperature (*24*–*27*), often leads to coupled GB sliding and migration, whereas pure sliding only occurs at relatively high temperatures (*5*–*7*). Unlike special, high-symmetry GBs (*4*–*7*), GBs in real polycrystals are commonly general types, i.e., low-symmetry bicrystallography, asymmetric GB planes, and non-flat GBs. It remains to be demonstrated whether the aforementioned atomic processes of GB sliding, as derived from highly idealized atomistic modeling and simulations, are directly applicable to general GBs in polycrystals under laboratory loading conditions.

We report in situ atomic-scale observations of sliding-dominated deformation of general high-angle tilt GBs in FCC Pt (bicrystals extracted from polycrystals) during nanomechanical testing (*28*, *29*) (fig. S1) in an aberration-corrected transmission electron microscope (Cs-TEM). The thin-film bicrystal geometry permits large-scale GB sliding without the constraints of the triple junctions present in polycrystals, thus facilitating step-by-step monitoring of GB sliding processes over a large sliding distance. We show a time series of in situ Cs-TEM images that provides a representative example of sliding by ~19 Å of an asymmetric <110>-tilt GB with a misorientation angle of 20.1° between adjoining grains (Fig. 1, A to H). A magnified Cs-TEM image of a segment of the initial GB shows that both the left (G_L) and right (G_R) grains are aligned with the <110> zone axis, such that white spots represent the projection of <110> atom-columns (Fig. 1I). General high-angle tilt GBs are rarely flat on the atomic scale. The commonly occurring asymmetric GBs (which are generally observed in real polycrystals) tend to form atomic-scale facets with atomic-sized steps (on one or both sides of the GB plane). For the GB segment studied (Fig. 1I), one side of the boundary exhibits flat, close-packed {111} facets on the face of grain G_R, whereas the other side involves an atomic-scale corrugation on the face of grain G_L, which is a reflection of the fact that this grain face is a high-index {331} plane of grain G_L. This corrugation can be described as single-atomic-layer height steps separated by {111} facets that are three to four atoms wide.

We characterized the structure of the GB (Fig. 1I) in terms of two sets of ½<110>{111} lattice dislocations residing at the GB that serve to accommodate the lattice misorientation between adjoining grains G_L and G_R across this asymmetric tilt GB. We marked each dislocation as "⊥" at the termination of its half plane. These dislocations often combined to form GB Lomer locks, each of which had a characteristic core structure of a five-membered unit (marked by a pentagon). Our Burgers loop analysis of a representative GB Lomer lock (Fig. 1J) shows its Burgers vector to be ½<110>{001} (fig. S2). During GB sliding, each Lomer lock adjusted its position and structure, frequently dissociating temporarily

[1]Institute of Microstructure and Property of Advanced Materials, Beijing Key Lab of Microstructure and Property of Advanced Materials, Beijing University of Technology, Beijing 100124, China. [2]Woodruff School of Mechanical Engineering, Georgia Institute of Technology, Atlanta, GA 30332, USA. [3]Department of Physics and Astronomy, Clemson University, Clemson, SC 29634 USA. [4]Shanghai Key Laboratory of Advanced High-Temperature Materials and Precision Forming, State Key Laboratory of Metal Matrix Composites, School of Materials Science and Engineering, Shanghai Jiao Tong University, Shanghai 200240, P. R. China. [5]Department of Materials Science and Engineering, Johns Hopkins University, Baltimore, MD 21218, USA. [6]Department of Materials Science and Engineering, City University of Hong Kong, Kowloon, Hong Kong SAR, China. [7]Department of Mechanical Engineering, The University of Hong Kong, Hong Kong SAR, China. [8]Department of Material Physics and Chemistry, University of Science and Technology Beijing, Beijing 100083, China. [9]Center for Alloy Innovation and Design (CAID), State Key Laboratory for Mechanical Behavior of Materials, Xi'an Jiaotong University, Xi'an 710049, China. [10]Beijing Institute of Artificial Intelligence, Faculty of Information Technology, Beijing Key Laboratory of Multimedia and Intelligent Software Technology, Beijing University of Technology, Beijing 100124, China. [11]College of Materials Science and Engineering, Chongqing University, Chongqing 40044, China. [12]Department of Materials Science, Zhejiang University, Hangzhou 310008, China. [13]International Digital Economy Academy (IDEA), Shenzhen, China.
***Corresponding author. Email: xdhan@bjut.edu.cn (X.D.H.); ting.zhu@me.gatech.edu (T.Z.); zezhang@zju.edu.cn (Z.Z.)**
†These authors contributed equally to this work.

into two individual ½<110>{111} dislocations that subsequently recombined into a Lomer lock. The large open space in the pentagon core unit of a GB Lomer lock facilitates the transfer of atom-columns across the GB plane.

To clarify the nature of atomic-scale GB sliding, we show high-magnification Cs-TEM images (Fig. 2) of the boxed GB region (Fig. 1A) (see movies S1 and S2 and figs. S3 and S4 for the complete time series). In these images, the in-plane atomic rows in G_R are indexed by numbers to facilitate tracking of changes in alignment between atomic rows in G_R and G_L across the GB due to its large sliding displacement (figs. S5 and S6). Image comparison (Fig. 2, A and B) reveals a series of pure GB sliding events. Before GB sliding (Fig. 2A), a close-packed {111} face of G_R was parallel to the GB plane and in contact with a stepped {331} face of G_L; the former consists of atom-columns labeled uppercase letters A to M, and the latter comprises atom-columns labeled lowercase letters a to o.

At 0 s, the step-corner atom-column i on the face of G_L was located at a bridge site relative to atom-columns J and K on the face of G_R (Fig. 2A). At 2.5 s, grain G_L slid such that this atom-column i translated to a neighboring bridge site (between columns I and J, Fig. 2B). Other atom-columns (lowercase letters) in the vicinity of column i also slid in a manner similar to that of rigid-body translation. The coherency of slip can also be seen by focusing on another step-corner atom-column g at a bridge site relative to columns H and I at 0 s, which translated to a bridge site relative to columns F and G at 2.5 s. Overall, atom-columns on the face of G_L slid in a rigid body motion relative to those on the face of G_R without rearranging the atomic structure of the faces of G_L and G_R (see fig. S6 for more details). This process was pure (or direct) GB sliding in the absence of GB migration. During this process, the pentagon core units of the GB Lomer locks adjusted their position and/or shape, with no discernable change in misorientation between adjoining grains G_L and G_R. Such pure sliding was mediated by disconnections that glide along the boundary plane (*4*).

In addition to pure GB sliding, we observed a previously unrecognized mode of coupled GB sliding and atomic plane transfer beyond 2.5 s. This GB deformation featured a change of the number of the {331} layers on the face of grain G_L on one side of the GB, which was a result of transfer of the constituent atom-columns of the {331} layers into the first {111} layer on the face of grain G_R on the other side of the GB, in conjunction with transport of transferred atom-columns along the boundary plane. Specifically, comparing GB atom-columns (uppercase and lowercase letters on grains G_L and G_R) at 0 s (Fig. 2A) and those (with mixed uppercase and lowercase letters on the face of grain G_R) at 6.0 and 9.0 s (Fig. 2, C and D), it can be seen that the transfer of atom-columns occurred predominantly from grain G_L to G_R. Focusing on a GB segment at 0 s (Fig. 2A), where the face of grain G_L consisted of the first-layer atom-columns g, i, and l and the second-layer columns f, h, and k, we see that these two atomic layers were closely spaced {331} planes (indicated by red dashed lines). At 6.0 and 9.0 s (Fig. 2, C and D), the constituent atom-columns in the two {331} layers were transferred across the boundary plane and inserted into the first {111} layer on the face of grain G_R (*29*) (fig. S7). This process is evident by the mixed uppercase and lowercase letters in Fig. 2D. Correspondingly, the two {331} layers on the face of G_L present at 0 s were removed by 9 s, thus reducing the number of lattice planes parallel to the GB plane and resulting in a normal displacement of grain G_L by two {331} interlayer spacings toward the GB plane. The coupled GB sliding and atomic plane transfer contrast with the commonly studied GB sliding deformation in previous experiments and simulations in which the number of lattice planes parallel to the GB plane was conserved.

To resolve the unit events of GB sliding more clearly than is possible through visual inspection, we developed an automated atom-column tracking method based on previous related studies (*29*–*32*). This method can automatically label atom-columns and thus correlate them between images during GB sliding (fig. S8 and movie S2). To demonstrate its efficacy, we first focused on cases in which the number of atom-columns was not conserved after atom-column transfer across the GB. For example, atom-column H was present at 2.5 s (Fig. 2B) but disappeared at 6 s (Fig. 2C); h′ appeared at 6 s but did not exist at 2.5 s. We were able to resolve the detailed formation process of h′ (Fig. 3) through automated atom-column tracking. At 5 s (Fig. 3A), atom-column h was located at the pentagon core unit of a GB Lomer lock. This core unit enclosed a relatively large free space, which can be considered a vacant lattice site on the face of grain G_R. At 5.5 s (Fig. 3B), a white streak appeared at h during its transfer. This streak was likely caused by the transient processes of transfer of individual atoms that belonged to the same atom-column h, but experienced nonuniform in-plane displacements due to kink nucleation and migration along the atom-column direction (*22*). At 6.0 s (Fig. 3C), h was transferred into the vacant site; meanwhile, a new atom-column h′ appeared at the site occupied previously by the transferred h. Although the total number of atoms should be conserved during GB sliding, the number of

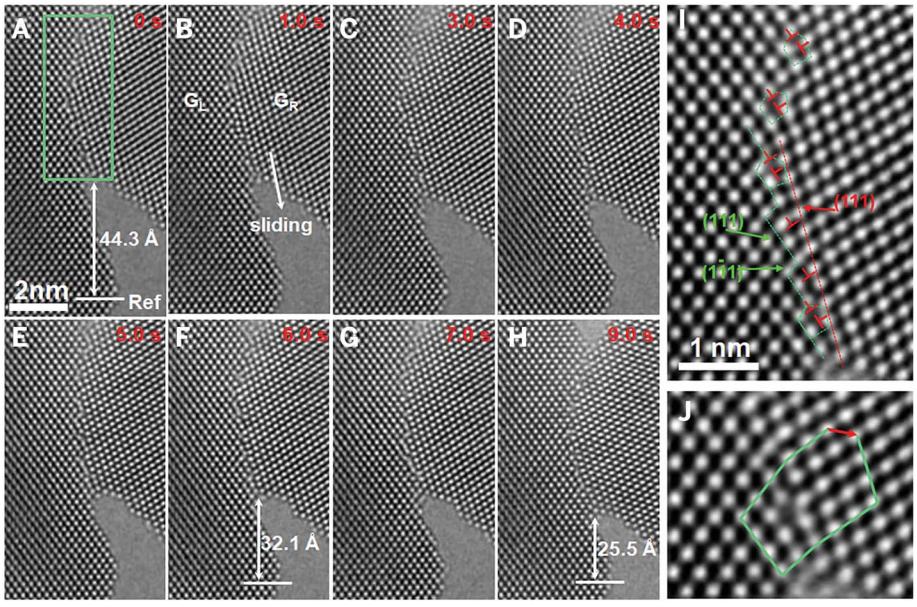

Fig. 1. Atomic-scale sliding of an asymmetric tilt GB in a Pt bicrystal. (**A** to **H**) Series of Cs-TEM images showing the sliding of an asymmetric <110>-tilt GB with 20.1° misorientation. The left and right grains are marked as G_L and G_R, respectively. (**I**) Magnified Cs-TEM image for the green boxed region in (A). One side of the boundary is the close-packed {111} face (marked by a red dashed line) of grain G_R, and the other side consists of a series of atomic-scale steps (marked by green dashed lines) on the face of grain G_L. Two sets of ½<110>{111} GB dislocations are identified, and the extra half plane of each dislocation is marked by symbol "⊥." These GB dislocations often combine to form GB Lomer locks, each of which has the characteristic core structure of a five-membered unit (marked by a pentagon). (**J**) Burgers loop analysis of a representative GB Lomer lock gives the Burgers vector of ½<110>{001} (red arrow).

atom-columns was increased during the transfer of h (fig. S9). The formation of h′ was further confirmed by the automated tracking of atom-column trajectories, as shown by an atom-column displacement map (Fig. 3D). Atoms in the newly formed atom-column h′ might come from atom-column h and/or its surrounding atom-columns through atom diffusion, but we could not determine this unambiguously from the Cs-TEM images. The diffusive processes of atom transport are likely mediated by vacancy migration. We obtained the map of atomic volume strains at 5 s (Fig. 3E) (*29*). The pentagon core unit of the GB Lomer lock exhibits a large local volume expansion, indicative of a sliding-induced increase of local expansion at this core unit that facilitates the transfer of h. This result implies that the appearance of new atom-columns or the disappearance of preexisting atom-columns (figs. S6 to S11) can effectively accommodate local deformation incompatibilities associated with stepped grain faces, thereby preventing the formation of energetically costly void formation or atom-column jamming at the GB. Therefore, the pentagon core unit of the GB Lomer lock plays an important role in the transfer of atom-columns and the associated formation and removal of atom-columns in the GB region.

To understand how the transfer of two {331} layers on the G_L face occurred through the transfer of constituent atom-columns during GB sliding, we identified a series of unit processes of atom-column transfer across the boundary plane with the aid of GB Lomer locks and subsequent atom-column transport along the GB (*29*) (Fig. 4 and fig. S12). As an example, we focused on the transfer of atom-column E from the face of G_L to G_R. At 4 s (Fig. 4A), we observed two GB Lomer locks in the form of pentagon core units: The top unit was E-f-F-S-T and the bottom was J-l-K-U-V. As GB sliding proceeded, grain G_R moved downward relative to grain G_L. Comparison of Fig. 4, B and C, shows that a vacant lattice site formed between atom-columns R and S such that the top pentagon core unit moved into the first {111} layer of the G_R face. This was followed by the transfer of atom-column E into the newly formed vacant site (fig. S12, A to D), resulting in the motion of the top pentagon core unit back to the G_L face. Although atom-column E left the G_L face, it did not disappear and was actually transferred to the first {111} layer on the G_R face. During the subsequent sliding of grain G_R, atom-column E was moved downward (fig. S12, D to F), resulting in its transport along the GB. We observed similar processes from the bottom pentagon core unit. In this case, atom-column l from the G_L face was first transferred into the first {111} layer of the G_R face (Fig. 4B) and then transported (Fig. 4C and fig. S12, D to F) in the same manner as atom-column E with the aid of the bottom pentagon core unit. As this type of atom-column transfer and motion repeated, several atom-columns were relocated from the {331} layers on the G_L face to the {111} layer on the G_R face (one by one) and then transported down the GB. These processes collectively resulted in the transfer of two {331} layers from the G_L face, leading to the mixing of atom-columns labeled by uppercase and lowercase letters on the G_R face (compare Fig. 2, A and D). Evidently, the coupled processes

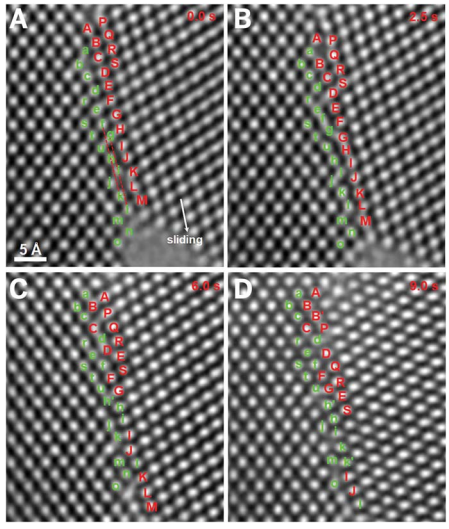

Fig. 2. Atomically resolved sliding at an asymmetric <110>-tilt GB. (**A** to **D**) Magnified Cs-TEM images (corresponding to the green boxed region in Fig. 1A) at 0, 2.5, 6.0, and 9.0 s, showing direct sliding along the boundary plane as well as sliding with atom-column transfer across the boundary plane resulting in coupled GB sliding and atomic plane transfer. At 0 s in (A), atom-columns on the face of grain G_L are marked by green lowercase letters, and atom-columns on the face of grain G_R by red uppercase letters. Two {331} layers on the face of grain G_L are indicated by red dashed lines and they are in contact with the close-packed {111} layer on the G_R face. At 9 s in (D), the two {331} layers were removed from the G_L face; the constituent atom-columns were transferred into the first {111} layer on the G_R face such that they were mixed with atom-columns therein.

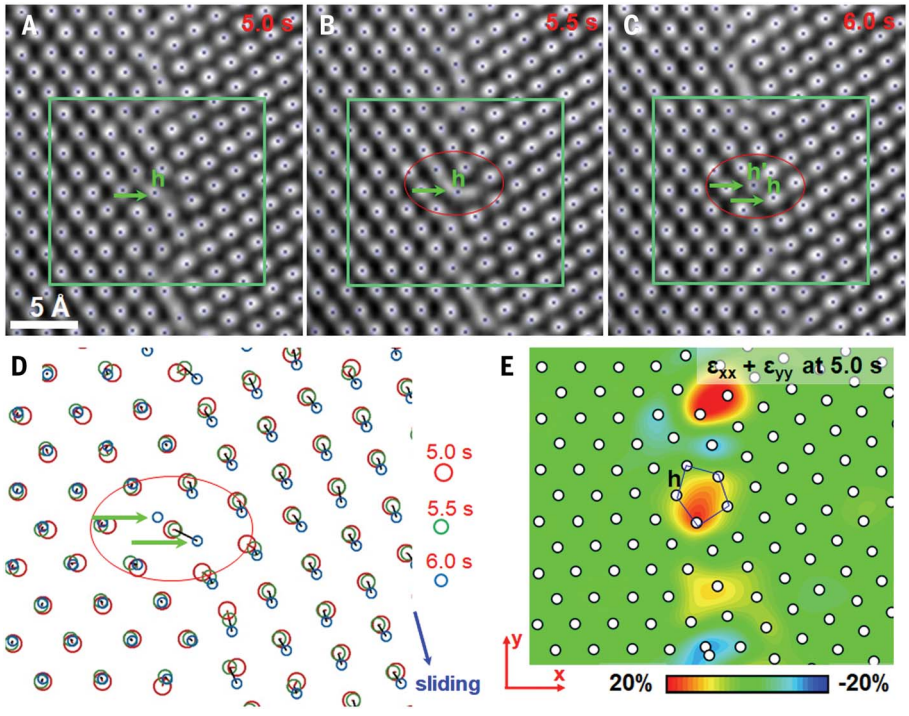

Fig. 3. Automated tracking of atom-column trajectories. (**A** to **C**) Cs-TEM images showing the transfer of atom-column h from the face of grain G_L to the close-packed face of grain G_R, accompanied by the appearance of a new atom-column labeled h′ in (C). Black dots in these images correspond to atom-column centers identified from automated analysis. (**D**) Atom-column trajectories and associated atomic displacement map extracted from (A) to (C) in the green boxed region from automated analysis. Atom-columns at different times are represented by circles of different sizes and colors. Each short segment represents the displacement vector of an atom-column between two consecutive images in (A) to (C), and the length of each segment represents the magnitude of the displacement. The green arrows indicate the transferred atom-column h and the newly formed atom-column h′, respectively. (**E**) Contour map of in-plane atomic volume strains $\varepsilon_{xx} + \varepsilon_{yy}$ at 5 s, calculated in reference to atom-column positions at 4.5 s.

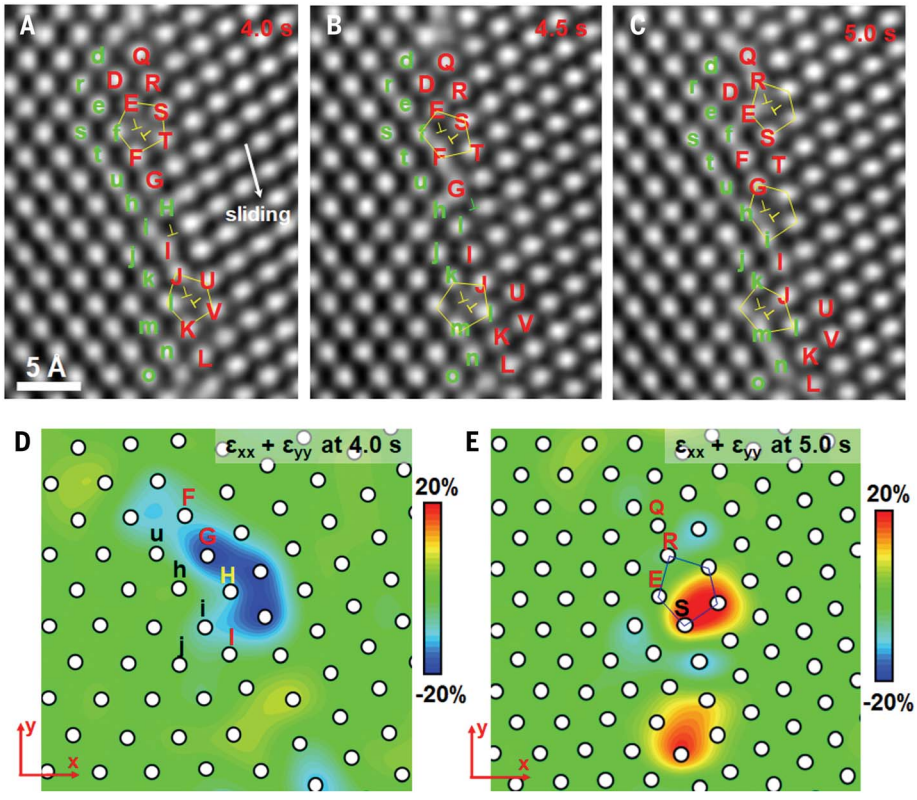

Fig. 4. Movement and formation of GB Lomer locks. (**A**) Two GB Lomer locks were identified from their respective core units (marked by pentagons), along with a stand-alone disconnection in between the two Lomer locks. (**B** and **C**) Movement of the top GB Lomer lock into the face of grain G_R occurred through the formation of a vacant lattice site between atom-columns R and S in (C). A new GB Lomer lock with a pentagon core unit formed in (C) by combining the stand-alone disconnection (marked by unpaired "⊥") in (A) and (B) and a disconnection gliding into the GB segment in the viewport. (**D** and **E**) Contour map of in-plane atomic volume strains $\varepsilon_{xx} + \varepsilon_{yy}$ at 4 and 5 s, respectively.

of GB sliding and atomic plane transfer occurred through a series of displacive events of atom-column transfer and motion.

Comparison of Fig. 4, B and C, reveals that disconnections glided along the GB. Such disconnections were short-lived during GB sliding because of the high stresses applied. Nonetheless, we captured a disconnection (Fig. 4C) due to its combination with a preexisting (intrinsic) GB dislocations to form a new GB Lomer lock in between the top and bottom GB Lomer locks. Subsequent GB sliding led to the annihilation of this temporary lock such that the pentagon core unit decomposed and the preexisting GB dislocation (marked by "⊥") reappeared (fig. S12). This kind of GB Lomer lock formation and decomposition was associated with the displacive process of disconnection gliding and was observed frequently (figs. S11 and S12). In addition, from the map of atomic volume strains at 4 s (Fig. 4D) and 5 s (Fig. 4E), we found a large local volume compression around atom-column H (Fig. 4D) that promoted its removal (Fig. 4B). A large local volume expansion around atom-column s (Fig. 4D) resulted from the transfer of the top pentagon core unit (Fig. 4C). These results, together with those shown in Fig. 3E, underscore the important effects of large local volume strain on driving the formation, removal, and transfer of atom-columns at the GB. We reiterate that the coupled processes of GB sliding and atomic plane transfer occurred through a series of displacive atomic events at ambient temperature and were driven by the applied high stresses at the GB. This stands in contrast to conventional creep deformation of polycrystalline materials operated at elevated temperatures and low stresses, which can be attributed to long-range diffusion of atoms near or at GBs.

Our in situ experiments show that the above atomic-scale processes of GB deformation were also frequently observed at the pentagon core unit of GB Lomer locks from other asymmetric, <110>-tilt GBs with misorientation angles of 82.1° and of 82.7° (figs. S13 to S19). For GBs in polycrystals, the same type of GB structures are common; namely, one side of the GB is a close-packed plane in one grain, and the face of the abutting grain consists of a series of atomic-scale steps. Therefore, the general GB structures and their sliding processes that we observed are representative of a broad class of GBs in polycrystals. In addition, we observed similar atom-column processes during plastic deformation of the mixed type of twist and tilt GBs (fig. S20).

To evaluate the effect of applied loads on driving GB sliding (fig. S1), we conducted peak-pair analysis to determine (elastic) lattice strains near the GB. From the peak-pair analysis strain maps (fig. S21), we calculated the average shear strain (γ_{xy}) near the GB as ~1.5%. The corresponding shear stress was ~980 MPa with the shear modulus of 65.2 GPa for Pt (*33*). Such high shear stress is a substantial fraction of the ideal shear strength (~2.1 GPa) of a perfect Pt crystal (*34*). The average compressive normal strain near the GB was ~0.5% and the corresponding compressive stress was ~850 MPa with an elastic modulus of 170 GPa. The high shear stresses applied enabled GB sliding at room temperature (*35*), and the high compressive stresses drove the transfer of two {331} layers. These high-stress conditions are usually attainable in bulk nanocrystalline and ultra-fine-grained metals, where GB sliding can play an important role in plastic flow (*11*, *15*, *16*). Therefore, the atomic-scale GB deformation processes that we observed should be applicable to bulk nanocrystalline and ultra-fine-grained FCC metals.

Past research has revealed pure GB sliding as well as coupled GB sliding and migration (*1*–*14*). These processes preserve the number of lattice planes parallel to the GB plane. Our in situ atomic-resolution results not only confirm these known sliding modes, but also suggest the possibility of atomic plane transfer during GB sliding, leading to a change of the number of lattice planes parallel to the GB plane. The latter mode can be interpreted in terms of GB disconnection–mediated boundary deformation. A GB disconnection is generally associated with a Burgers vector **b** and a step height h (*7*). During GB sliding from 0 to 2.5s, the GB disconnections involved had a Burgers vector **b** along the GB plane without step component (fig. S22), resulting in pure GB sliding. During coupled GB sliding and atomic plane transfer, the GB disconnections involved had a Burgers vector **b** with both nonzero normal and tangential components with respect to the GB plane (fig. S22). The movement of this type of disconnections produced a GB sliding displacement along the GB plane as well as a relative displacement between adjoining grains normal to the GB plane. In addition, we found that GB atom-columns could be transferred from one side to the other and then moved along the boundary plane upon further GB sliding. This type of displacive motion of atom-columns by an appreciable distance is different from the conventional diffusional creep at elevated temperatures by vacancy-mediated long-range atomic diffusion.

The ability to track time-resolved, atomic-scale motion of GBs opens opportunities for gaining deeper insight into the mechanisms of GB sliding and the mechanical behavior of polycrystalline materials. Some of the observed atomistic mechanisms of sliding of general tilt GBs have not been reported previously. The present results clearly show how general GBs slide at low temperatures and with no (or very little) accompanying GB migration. Broadly, this work demonstrates the great potential of harnessing in situ atomic-resolution TEM experiments for understanding interface-mediated deformation and failure mechanisms in polycrystalline materials and provides new opportunities for high-resolution handshaking between experiment and atomistic modeling.

REFERENCES AND NOTES

1. A. P. Sutton, R. W. Balluffi, *Interfaces in Crystalline Materials* (Oxford Univ. Press, 1995).
2. T. Meiners, T. Frolov, R. E. Rudd, G. Dehm, C. H. Liebscher, *Nature* **579**, 375–378 (2020).
3. R. Raj, M. F. Ashby, *Metall. Trans., A, Phys. Metall. Mater. Sci.* **2**, 1113–1127 (1971).
4. M. F. Ashby, *Surf. Sci.* **31**, 498–542 (1972).
5. J. W. Cahn, Y. Mishin, A. Suzuki, *Acta Mater.* **54**, 4953–4975 (2006).
6. Y. Mishin, M. Asta, J. Li, *Acta Mater.* **58**, 1117–1151 (2010).
7. J. Han, S. L. Thomas, D. J. Srolovitz, *Prog. Mater. Sci.* **98**, 386–476 (2018).
8. J. Schiotz, F. D. Di Tolla, K. W. Jacobsen, *Nature* **391**, 561–563 (1998).
9. H. Van Swygenhoven, P. A. Derlet, *Phys. Rev. B Condens. Matter* **64**, 224105 (2001).
10. V. Yamakov, D. Wolf, S. R. Phillpot, A. K. Mukherjee, H. Gleiter, *Nat. Mater.* **3**, 43–47 (2004).
11. T. Zhu, J. Li, *Prog. Mater. Sci.* **55**, 710–757 (2010).
12. T. Chookajorn, H. A. Murdoch, C. A. Schuh, *Science* **337**, 951–954 (2012).
13. Z. Shan *et al*., *Science* **305**, 654–657 (2004).
14. T. J. Rupert, D. S. Gianola, Y. Gan, K. J. Hemker, *Science* **326**, 1686–1690 (2009).
15. X. W. Gu *et al*., *Nano Lett.* **12**, 6385–6392 (2012).
16. Z. H. Aitken, D. Jang, C. R. Weinberger, J. R. Greer, *Small* **10**, 100–108 (2014).
17. X. Zhang *et al*., *Science* **357**, 397–400 (2017).
18. J. Hu, Y. N. Shi, X. Sauvage, G. Sha, K. Lu, *Science* **355**, 1292–1296 (2017).
19. Q. Zhu *et al*., *Nat. Commun.* **11**, 3100 (2020).
20. M. Jin, A. M. Minor, E. A. Stach, J. W. Morris Jr., *Acta Mater.* **52**, 5381–5387 (2004).
21. P. Y. Huang *et al*., *Science* **342**, 224–227 (2013).
22. M. L. Bowers, C. Ophus, A. Gautam, F. Lançon, U. Dahmen, *Phys. Rev. Lett.* **116**, 106102 (2016).
23. A. Azizi *et al*., *Nat. Commun.* **5**, 4867 (2014).
24. H. Van Swygenhoven, J. R. Weertman, *Mater. Today* **9**, 24–31 (2006).
25. D. S. Gianola, D. Farkas, M. Gamarra, M. He, *J. Appl. Phys.* **112**, 124313 (2012).
26. E. R. Homer, S. M. Foiles, E. A. Holm, D. L. Olmsted, *Acta Mater.* **61**, 1048–1060 (2013).
27. S. L. Thomas, K. Chen, J. Han, P. K. Purohit, D. J. Srolovitz, *Nat. Commun.* **8**, 1764 (2017).
28. L. Wang *et al*., *Nat. Commun.* **8**, 2142 (2017).
29. Materials and methods are available as supplementary materials.
30. J. C. Crocker, D. G. Grier, *J. Colloid Interface Sci.* **179**, 298–310 (1996).
31. I. F. Sbalzarini, P. Koumoutsakos, *J. Struct. Biol.* **151**, 182–195 (2005).
32. C. Ophus, H. I. Rasool, M. Linck, A. Zettl, J. Ciston, *Adv. Struct. Chem. Imaging* **2**, 15 (2017).
33. D. H. Warner, W. A. Curtin, S. Qu, *Nat. Mater.* **6**, 876–881 (2007).
34. M. Cerny, J. Pokluda, *Comput. Mater. Sci.* **44**, 127–130 (2008).
35. N. Combe, F. Mompiou, M. Legros, *Phys. Rev. B* **93**, 024109 (2016).

ACKNOWLEDGMENTS

X.D.H. and L.W. acknowledge support by the Beijing Outstanding Young Scientists Projects (grant BJJWZYJH01201910005018), the Basic Science Center Program for Multiphase Evolution in Hypergravity of the National Natural Science Foundation of China (grant 51988101), the Beijing Natural Science Foundation (grant Z180014), and the Natural Science Foundation of China (grants 51771004, 51988101, and 91860202). **Author contributions:** L.W. and Y.Z. contributed equally to this work. X.D.H., T.Z., and Z.Z. designed the project and guided the research. L.W. conducted the in situ TEM experiments. Y.Z. developed the automated atom-column tracking method. L.W., H.Z., Y.Z., Zh.Z., J.H., G.Y., E.M., T.Z., D.S., X.X.H., X.D.H., and Z.Z. performed the analysis of TEM results. P.L., M.W.C., J.H., D.S., Y.Z.G., G.Y., D.L.K., Y.L.H., and B.C.Y. performed the peak-pair analysis strain mapping. J.T. synthesized the thin films. L.W., T.Z., E.M., D.S., and X.D.H. wrote the manuscript. All authors contributed to discussion of the results. **Competing interests:** The authors declare no competing financial interests. **Data and materials availability:** All data are available in the main text or the supplementary materials.

SUPPLEMENTARY MATERIALS

science.org/doi/10.1126/science.abm2612
Materials and Methods
Figs. S1 to S23
Table S1
References (*36*–*43*)

12 September 2021; accepted 16 February 2022
10.1126/science.abm2612